Communication

Comparative Study of Cold Sintering Process and Autoclave Thermo-Vapor Treatment on a ZnO Sample

Yurii Ivakin [1,2]**, Andrey Smirnov** [2,]*****, **Anastasia Kholodkova** [1] iD**, Alexander Vasin** [2]**, Mikhail Kormilicin** [2]**, Maxim Kornyushin** [2] **and Vladimir Stolyarov** [3]

1   Chemistry Department, M. V. Lomonosov Moscow State University, 119991 Moscow, Russia; ivakin@kge.msu.ru (Y.I.); anastasia.kholodkova@gmail.com (A.K.)
2   Mobile Solutions Engineering Center, MIREA-Russian Technological University, 119454 Moscow, Russia; alexandrvasin123@gmail.com (A.V.); kmihail2013@yandex.ru (M.K.); maksim.korn0312@yandex.ru (M.K.)
3   Department of Friction and Wear, Mechanical Engineering Research Institute of RAS, 101990 Moscow, Russia; vlstol@mail.ru
*   Correspondence: smirnov_av@mirea.ru

Abstract: Analysis of scanning electron microscopy images was used to study the changes in the crystal size distribution of ZnO, which occurred during its processing in an aqueous medium at 220–255 °C and an equilibrium vapor pressure in an autoclave. The results were compared with those of ZnO placed in a die for treatment under similar conditions supplemented with mechanical pressure application in the cold sintering process. In both cases, ZnO was treated in the presence of an activating additive: either zinc acetate or ammonium chloride. During autoclaving, a powder consisting of fine ZnO monocrystals was obtained, while the cold sintering process led to ceramics formation. Under vapor pressure and mechanical pressure, the aqueous medium affected ZnO transformation by the same mechanism of solid-phase mobility activation due to the additives' influence. The higher the content of additives in the medium, and the higher the mechanical pressure, the more pronounced activating effect was observed. Mass transfer during the cold sintering process occurred mainly by the coalescence of crystals, while without mechanical pressure, the predominance of surface spreading was revealed. In the initial ZnO powder, the average crystal size was 0.193 μm. It grew up to 0.316–0.386 μm in a fine-crystalline powder formed in the autoclave and to an average grain size of 0.244–0.799 μm in the ceramics, which relative density reached 0.82–0.96. A scheme explaining the influence of an aqueous medium on the solid-phase mobility of ZnO structure was proposed. It was found that the addition of 7.6 mol% ammonium chloride to the reaction medium causes the processes of compaction and grain growth similar to those observed in ZnO Cold Sintering Process with the addition of 0.925 mol% zinc acetate.

Keywords: oxide ceramics; zinc oxide; cold sintering process; thermo-vapor treatment; solid-phase mobility in a water medium; crystal size distribution; coalescence; surface spreading

1. Introduction

Recent studies have shown that the sintering temperatures of oxide ceramics in the presence of water decrease from the region above 1000 °C to the range of 200–400 °C [1,2]. The sintering of dense ceramics of simple and complex oxides at a low temperature due to the presence of water is called the cold sintering process (CSP) [3]. For example, the sintering temperature of ZnO ceramics is lowered by hundreds of degrees (from >1000 °C to <200 °C), and the sintering time is significantly reduced. It was found [4,5] that the presence of acetates contributes to the sintering of ZnO. In [6], the CSP of ZnO ceramics was carried out at a temperature of 240 °C in a medium of 20% acetic acid solution (1.6 mol% CH_3COOH by weight of ZnO). To explain the effect of the acidic medium of an aqueous solution on mass transfer during sintering, the idea of the dissolution of stressed areas and the release of ZnO in the contact region of particles is usually used [7–12]. When

discussing the results of CSP in several works [7,13–16], the insufficiency of the dissolution-reprecipitation mechanism for understanding the processes occurring during sintering of oxides with the participation of water is noted. The necessity of searching for scientific bases for the choice of activating additives for various oxide materials is also justified [7].

Additional information about the processes occurring in the interaction of simple and complex oxides with the water medium is provided by studies of transformations under hydrothermal or thermo-vapor conditions of autoclave treatment (TVT). First of all, it should be noted that when processing occurs in a water medium in an autoclave without applying mechanical pressure, a sharp decrease in the temperature of oxide transformations is also observed (Table 1). In studies of the synthesis and changes in the dispersion of simple and complex oxides in water vapor, as well as in the medium of sub- and supercritical water fluid [17–19], ideas have been formed about the mechanisms of the processes that can be used to interpret the effect of mechanical pressure on the mass transfer processes during cold sintering.

Table 1. Influence of the aquatic environment on the oxide's transformations temperature.

Transformation			Without Water, °C	TVT in the Aquatic Environment, °C
$2Al(OH)_3$	→			
$2AlOOH$	→	$\alpha\text{-}Al_2O_3$	1100–1200 [20]	400 [21–23]
$ZnO + Al_2O_3$	→	$ZnAl_2O_4$	800 [24]	180 [25]
$BaO + TiO_2$	→	$BaTiO_3$	1300 [26]	200 [17]
$MgO + Al_2O_3$	→	$MgAl_2O_4$	1400 [27,28]	400 [29]
ZnO	→	recrystal. ZnO	650–750 [30]	100 [19]

In this work, the effect of two activating additives—zinc acetate ($Zn (CH_3COO)_2 \cdot 2H_2O$) and ammonium chloride (NH_4Cl)—on the recrystallization of ZnO during autoclave treatment in water vapor under free powder filling conditions and under CSP in a similar environment, but with the application of mechanical pressure, was studied. The selection of adjuvants was made based on results of experiments on recrystallization of ZnO to the source powder in the environment of water vapor at temperatures of 100–400 °C (TVT) in the presence of activator located on the surface of particles or in water vapor, which leads to a change of dispersion with the formation of fine crystalline ZnO powder [19]. Activation of the transformation occurs when zinc chloride and ammonium chloride are applied to the surface of ZnO particles [19] or the hydrolysis products of chlorides, acetates, and crystalline iodine are transferred to the water vapor medium [19], which are placed with water on the bottom of the autoclave outside the container with dry ZnO powder. The activating agent is the corresponding volatile acid. The interaction of acid protons with ZnO leads to an increase in hydroxyl groups' concentration in its structure, formed during the dissociative adsorption of water molecules from the environment. Hydroxyl groups do not form stable compounds with ZnO under TVT conditions [19,31,32] and are released into the gas phase, forming water molecules. The intensive transition of water molecules from the gas medium to the ZnO structure and back leads to numerous local rearrangements and the formation of defects in the crystal structure, which determine the appearance of solid-phase mobility. Due to the different frequency of local rearrangements of the oxide matrix, structural positions with an increased lifetime (the time between the appearance of the position and its rearrangement during the exchange of water molecules with the medium) accumulate, and the crystal lattice is improved [17–19]. As a result, an ordered ZnO structure is formed with a smooth surface of well-cut crystals. Also, in the medium of water vapor or water fluid, during prolonged exposure of the formed fine crystalline ZnO, there is a redistribution of mass, and a change in the powder's disperse composition, i.e., recrystallization occurs [19]. A dense ceramic structure is formed during mechanical uniaxial pressing of ZnO powder in a low-density water-acetate medium [6,33].

The present work aims to investigate the effect of mechanical pressure on the change in the dispersion of ZnO powder during processing in water vapor in the presence of various additives that activate mass transfer between crystals. It is assumed that the determination of micro additives' activity in the processes of mass redistribution under conditions of increased temperature and pressure of the water medium in the autoclave can contribute to the optimization of the water medium composition and the CSP conditions of oxide ceramics.

2. Materials and Methods

In the present work was used dispersed fine crystalline ZnO powder with an average particle size of 0.193 µm, zinc acetate ($Zn(CH_3COO)_2 \cdot 2H_2O$), and ammonium chloride (NH_4Cl). All reagents had a content of the main component of more than 99%.

For ZnO preparation with the applied activator, 20 g of the powder was mixed in an ultrasonic bath with 30 mL of the activator solution in distilled water. The suspension was dried at a temperature not exceeding 70°C for 12 h. Then the dried mass was crushed in an agate mortar and sifted through a sieve with holes of 300 µm.

CSP was carried out in a steel mold with induction heating (Figure 1). The advantage of induction heating is a higher heating rate and less thermal inertia of the structure. However, this heating method is less manageable in setting the set temperature values. The mold contained four punches (with a diameter of 17 mm), between which ZnO powder was located in the middle, and between the other punches, the Teflon seals rings were placed. The seals were used to prevent water from squeezing out and evaporating through the gaps in the mold during the pre-compaction of the mixture for 1 h at a pressing pressure of 396 MPa. Two grams of ZnO powder were poured into the mold with the lower pair of punches and 0.4 mL of water was added with careful mixing (20% of the mass of ZnO). Then the second pair of punches was lowered into the mold. A hot junction of the thermocouple was fixed to the mold in a recess near the sample. The mold with the heater was installed along the axis of the hydraulic press. The powder's shrinkage in the mold was controlled by measuring the axial displacement of the lower platform of the hydraulic press with a mechanical movement indicator of the clock type (with a division price of 10 µm) fixed on a fixed frame. The CSP modes and compositions of the initial mixtures are presented in (Table 2).
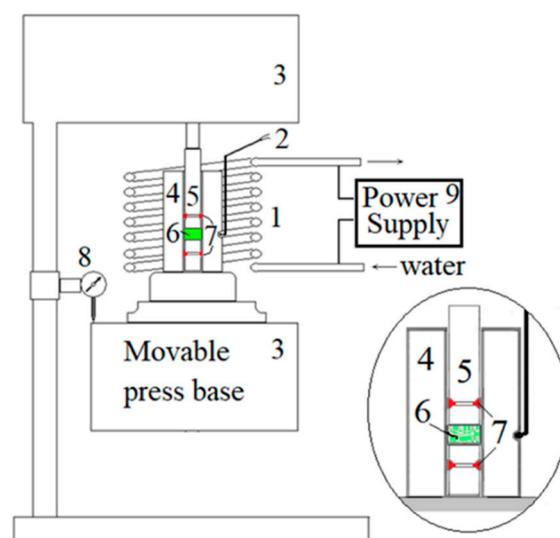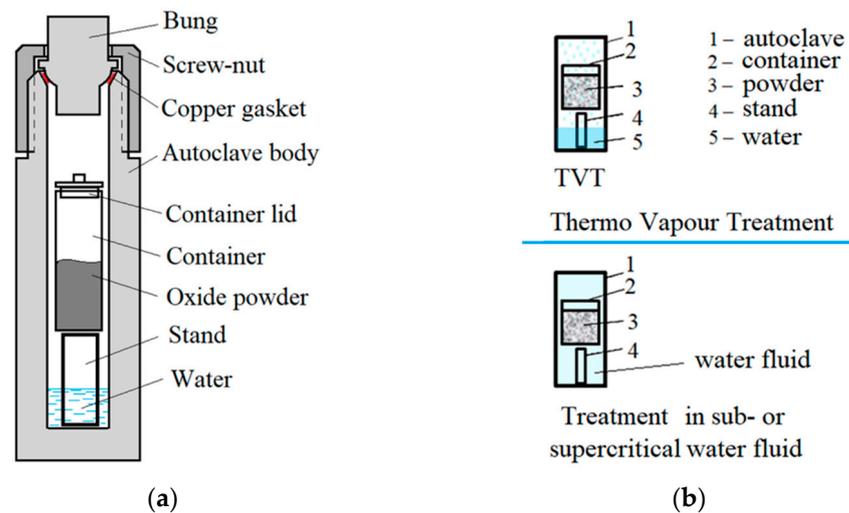

Figure 1. The CSP setup: 1—coil induction heater; 2—thermocouple; 3—hydraulic press; 4—die mold; 5—set of punches; 6—ZnO powder; 7—seal rings; 8—motion sensor; 9—Power Supply.

Table 2. The CSP conditions.

Sample #	Additive; mol%	Pressing (Compaction, 1 h), MPa	Pressing (Dwell), MPa	TDwell, °C	Dwell Time, min
CSP1	$Zn(Ac)_2 \cdot 2H_2O$; 0.185	396	77	220	60
CSP2	$Zn(Ac)_2 \cdot 2H_2O$; 0.927	396	77	255	60
CSP3	NH_4Cl; 4.56	396	396	246	60
CSP4	NH_4Cl; 7.6	396	396	255	60

TVT of ZnO powder was performed in laboratory autoclaves with a volume of 17 mL with a copper sealing gasket and using Teflon containers with a lid on a free fit. The container was installed in an autoclave on a stand. Water was poured into the bottom of the autoclave below the container on the stand. A sample of ZnO powder with an activator applied by impregnation to the particles' surface was placed in the container. At such loading of the autoclave, heating and isothermal ZnO holding took place in water vapor or in sub- and supercritical water fluid and corresponded to the conditions of TVT (Figure 2). The features of filling the autoclave with water are described in [19]. The conditions for processing zinc oxide in an autoclave are presented in Table 3. The additive content in the reaction medium was calculated in molar percentages relative to the mass of ZnO.

Figure 2. The TVT setup: (**a**)—autoclave scheme; (**b**)—differences between TVT and sub- or supercritical water fluid treatment.

Table 3. The TVT conditions.

Sample #	Additive; mol%	Water Inside the Container; mL	Water Outside Container; mL	Vapor Pressure; MPa	T; °C	Dwell Time; h
TVT1	$Zn(Ac)_2 \cdot 2H_2O$; 0.185	-	1	3.46	240	26
TVT2	$Zn(Ac)_2 \cdot 2H_2O$; 0.927	-	1	3.46	240	24
TVT3	NH_4Cl; 4.56	-	1	3.46	240	14
TVT4	NH_4Cl; 7.6	-	1	3.46	240	14

The relative density of ceramics was determined by the Archimedean method. The morphology of ceramic powders and chips was studied using a JSM-6390 LA scanning electron microscope (JEOL Ltd., Tokyo, Japan). The size distribution of powder crystals and grains of CSP ceramic samples was determined by analyzing images [18] obtained with a scanning electron microscope (SEM). The average size of crystals and grains was determined by simply averaging over all measured objects in the sample. The Image-Pro software was used to determine the size of 2000 to 3000 particles in each sample. Due to

a large number of measured particles, the measurement error was less than 1% (Table 4). The phase composition of the samples was studied on an XRD-6000 X-ray diffractometer (Shimadzu Corp., Kyoto, Japan) with CuKα radiation and the wavelength of the secondary radiation (λ = 1.54 Å) with a graphite monochromator in the range of $20° \leq 2\theta \leq 70°$ with step $2\theta = 0.02°$. The voltage is 50 kV, the cathode glow current is 250 mA. Scanning speed 5°/min. The samples phases composition was determined by comparing the experimental data with the data of the PDF-2 database.

3. Results

Figure 3 shows the SEM image and the crystal size distribution of the initial ZnO powder. The total average crystal size is 0.193 μm. These results are used as initial data for evaluating the processes of crystal growth in TVT and densification and grain growth in CSP.

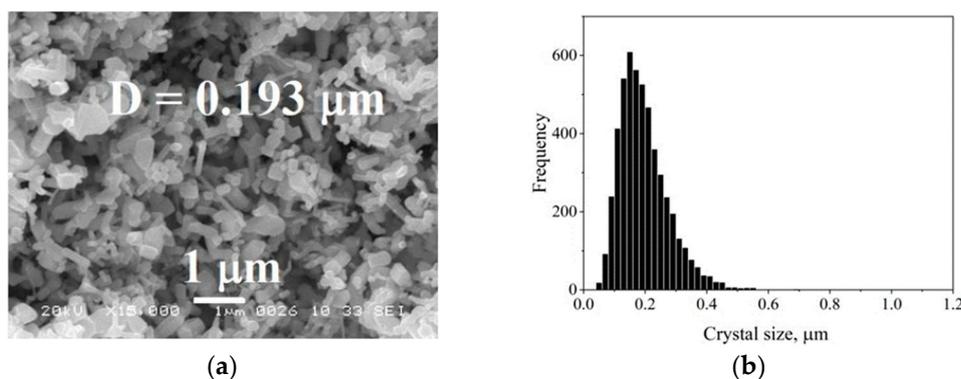(a)   (b)

Figure 3. Characteristics of the initial ZnO powder: (**a**) SEM micrograph (Reprinted from Ref. [33], copyright (2019), with the kind permission of Springer Nature.); (**b**) crystal size distribution.

Figure 4 shows a comparison of SEM images of microstructure of samples CSP1 and CSP2 obtained in the CSP and samples of powders TVT1 and TVT2 obtained in TVT with an identical amount of zinc acetate.

Comparing the analysis results of the microstructure of CSP and TVT of ZnO samples with the addition of ammonium chloride is shown in Figure 5. The distribution of particle sizes in the samples obtained by TVT and the grain sizes of CSP samples is shown in Figure 6.

Figure 7 shows X-ray patterns of samples obtained in a medium of zinc acetate-sample CSP1 (a) and the presence of an additive of 7.6 mol% NH_4Cl—sample CSP4 (b), as well as sample TVT4 (c). The X-ray pattern of sample CSP1 in the range $2\theta = 10$–$70°$ contains only characteristic reflexes of the ZnO structure of wurtzite. There are no extraneous reflexes (Figure 7a). The X-ray pattern in Figure 7c refers to the TVT4 sample with the same amount of ammonium chloride added in the CSP4 sample. In addition to the ZnO reflexes, low-intensity reflexes are visible, which, as in [19], belong to the $Zn_5(OH)_8Cl_2H_2O$ (JCPDS 7-155) phase, formed after TVT ZnO at 240 °C (Table 3). The appearance of the $Zn_5(OH)_8Cl_2H_2O$ phase with a decomposition temperature of 250 °C was observed in [34] and also in [10]. On the X-ray pattern of the CSP4 sample (Figure 7b), unidentified traces of the decay product of this phase are marked with a round icon.
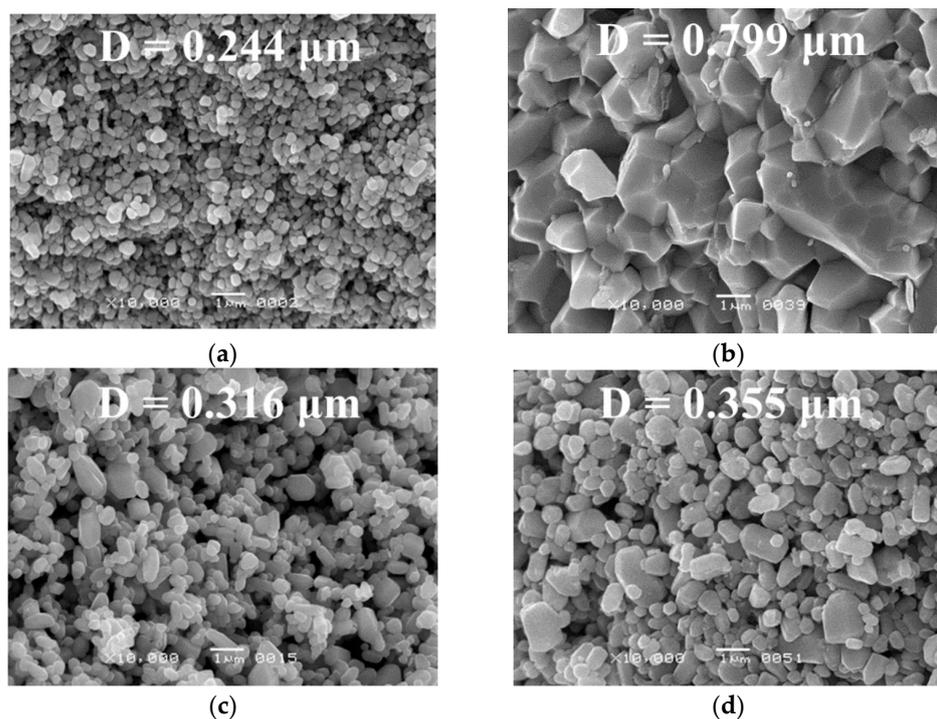
Figure 4. Microstructure of samples obtained in an acetate medium: (**a**) CSP1 sample (0.185 mol% $Zn(Ac)_2$); (**b**) CSP2 sample (0.927 mol% $Zn(Ac)_2$) (Reprinted from Ref. [33], copyright (2019), with the kind permission of Springer Nature.); (**c**) TVT1 sample (0.185 mol% $Zn(Ac)_2$); (**d**) TVT2 sample (0.927 mol% $Zn(Ac)_2$).
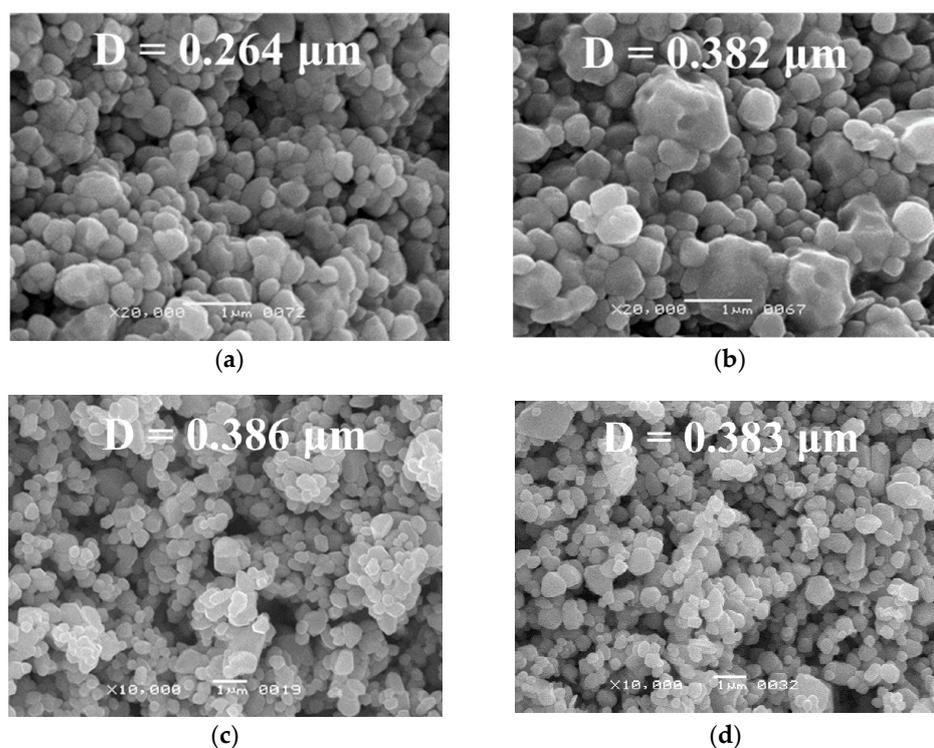

Figure 5. Microstructure of CSP and TVT samples, additive-ammonium chloride: (**a**) CSP3 sample (4.56 mol% NH_4Cl); (**b**) CSP4 sample (7.6 mol% NH_4Cl); (**c**) TVT3 sample (4.56 mol% NH_4Cl); (**d**) TVT4 sample (7.6 mol% NH_4Cl).
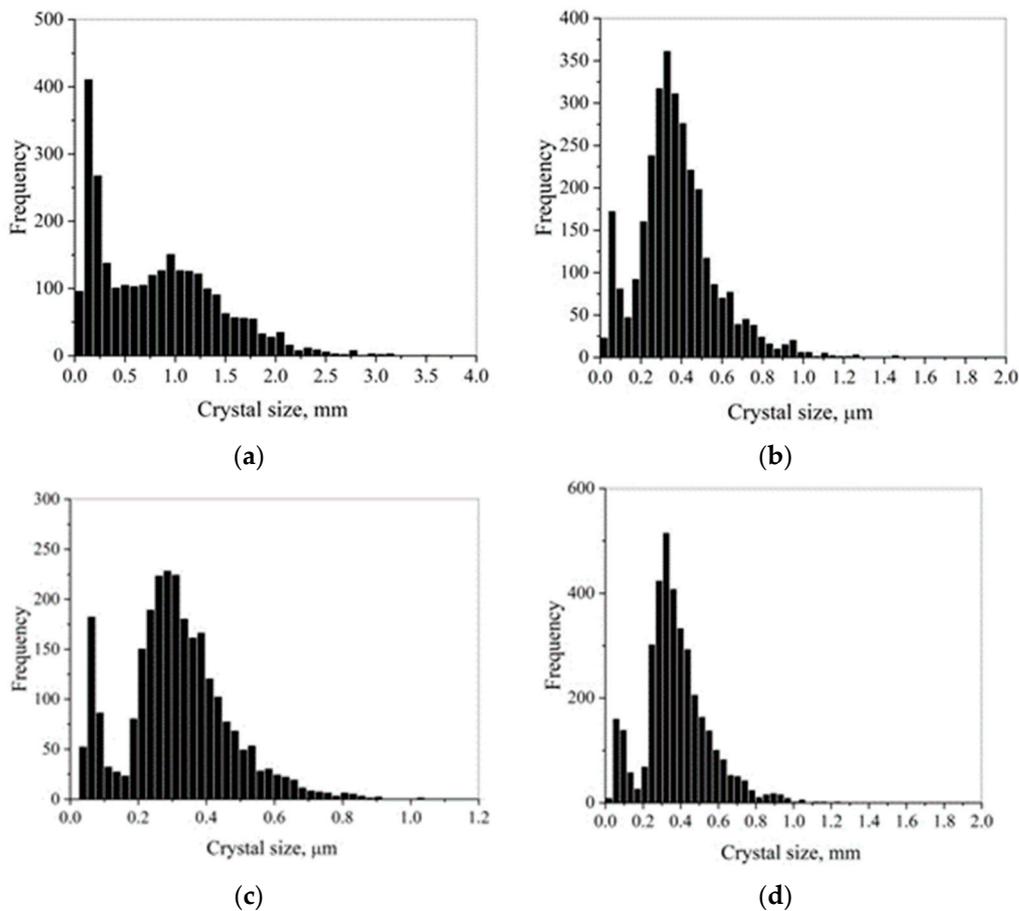
Figure 6. Grain size distribution of samples after CSP and crystals size distribution after TVT: (**a**) CSP2 (0.927 mol% Zn(Ac)$_2$); (**b**) CSP4 (7.6 mol% NH$_4$Cl); (**c**) TVT2 (0.927 mol% Zn(Ac)$_2$); (**d**) TVT4 (7.6 mol% NH$_4$Cl).

Figure 7. X-ray patterns of samples: (**a**) CSP1; (**b**) CSP4; (**c**) TVT4: black—full spectrum; green—the spectrum is shown with increased sensitivity for the low-intensity reflexes detection; green dots—reflexes of unidentified phase.

The results of the experiments are summarized in Table 4. For CSP samples, data on the relative density and average grain size are given. For TVT samples, data on the average crystal size are presented.

Table 4. The experimental results.

Sample	Additive; mol%	Mean Grain Size, μm	Relative Density
CSP1	$Zn(Ac)_2 \cdot 2H_2O$; 0.185	0.244 ± 0.002	0.83 ± 0.02
CSP2	$Zn(Ac)_2 \cdot 2H_2O$; 0.927	0.799 ± 0.011	0.96 ± 0.02
CSP3	NH_4Cl; 4.56	0.264 ± 0.002	0.82 ± 0.02
CSP4	NH_4Cl; 7.6	0.382 ± 0.004	0.91 ± 0.02
Sample	**Additive; mol%**	**Mean Crystal Size, μm**	
TVT1	$Zn(Ac)_2 \cdot 2H_2O$; 0.185	0.316 ± 0.003	
TVT2	$Zn(Ac)_2 \cdot 2H_2O$; 0.927	0.355 ± 0.004	
TVT3	NH_4Cl; 4.56	0.386 ± 0.003	
TVT4	NH_4Cl; 7.6	0.383 ± 0.003	

4. Discussion

A comparative study of the effect of activating additives on the CSP and TVT processes of fine-crystalline ZnO powder was carried out based on the hypothesis of similarity of the two processes' conditions under consideration. The CSP3 sample obtained at CSP with the addition of 4.56 mol % NH_4Cl in a mold with Teflon sealing rings had a residual moisture content of 0.2% (residual water weight 0.0034 g). In a dry sample with a mass of 1.6582 g and a relative density of 0.82, the volume of the gaps between the crystals is 0.065 cm^3. At 250 °C, 0.0013 g of water evaporates into the interstices' volume in the form of saturated steam [35]. The remaining 0.0021 g of water occupies 4% of the volume of the gaps. Thus, when the working volume is reduced during pressing, the main part of the initially added water (0.4 mL) is squeezed out, and the powder is compacted in a water vapor environment. Due to this, the interaction of ZnO with water vapor at TVT in an autoclave and CSP in a mold with Teflon sealing rings occurs under similar conditions, except for the influence of mechanical pressing pressure.

Figure 4 compares the SEM images and the size distribution of ceramics' cleavage zones after CSP and crystals after TVT. The crystals of the TVT1 sample are noticeably larger than the grains on the CSP1 ceramic chip, but in both cases have a similar morphology of rounded particles. At the same time, the grains in the CSP1 sample grew and acquired a rounded morphology in just 1 h at a temperature of 220 °C and a pressing pressure of 77 MPa, and the crystal growth time of the TVT1 sample was 26 h at a temperature of 240 °C and a water vapor pressure of 3.46 MPa. This result indicates that the level of activator content of 0.185 mol% zinc acetate in the reaction medium was sufficient for slow mass transfer but insufficient for the appearance of structure mobility, at which it is possible to fill the space with the formation of a forced cut of crystalline grains of ceramics. A comparison of the microstructure of the cleavage of the CSP2 sample and the morphology of the crystals of the TVT2 sample obtained at 0.927 mol% zinc acetate shows that the increased content of the activator in the reaction medium led to almost complete filling of the space with the formation of a forced grain cut (average size 0.799 μm) and obtaining ceramics with a high relative density (0.96; Table 4). The mechanism of rapid mass transfer between crystals with a mobile structure is coalescence. The pressing pressure of 77 MPa and a temperature of 255 °C for 60 min were sufficient for consolidation under the influence of a sufficient amount of zinc acetate and water vapor. Under TVT ZnO conditions with 0.927 mol% zinc acetate at a temperature of 240 °C and a water vapor pressure of 3.46 MPa, the crystals grew to an average size of 0.355 μm in 24 h, which is significantly inferior to the average grain size in the CSP2 sample but exceeds the average crystal size of the TVT1 sample. Consequently, in a water vapor medium at temperatures of 220–255 °C, a slow mass transfer occurs, the mechanism of which under the influence of mechanical pressure turns into coalescence.

It should be noted that a similar slow mass transfer between ZnO crystals was observed when the samples were stored in a humid atmosphere at room temperature [36–38] and 85 °C [39]. According to our ideas, the change in the dispersion of ZnO powder during storage in a humid atmosphere or application of an additive from an aqueous solution is

explained by the mobility of the crystal structure in a water medium [19]. An increase in mass transfer with an increase in the additive content when zinc acetate is applied indicates an increase in the mobility of the structure of ZnO crystals.

Figure 5 shows the results of CSP and TVT of ZnO with NH_4Cl additive. The ceramics fractures run along the boundaries between the grains and reveal their morphology. SEM images of CSP and TVT samples show that the bulk of crystals and grains have the same morphology of rounded particles. The TVT3 sample crystals have smooth faces of regular cut and are noticeably larger than the grains of the CSP3 sample. CSP3 ceramic grains are less isometric and can form dense agglomerates with narrow boundaries. With an increase in the additive concentration from 4.56 mol% to 7.6 mol%, the larger grains of the CSP4 sample acquire a forced cut with traces of neighboring small spherical crystals (Figure 5b). Such crystals with forced cut correspond to the initial stage of growth of ceramic grains. They are formed with the disappearance of boundaries in a dense agglomerate due to the coalescence of neighboring crystals with a mobile structure and flow around crystals with their low mobility. Thus, the compacted microstructure of the CSP 3 sample is formed by changing the shape of grains with a mobile structure. With an increase in the content of the additive from 4.56 mol% to 7.6 mol% NH_4Cl the threshold of the crystal structure mobility is overcome, and coalescence begins, the grain size of ceramics changes (Figure 5b), the density of ceramics increases (Table 4). Thus, when 7.6 mol% NH_4Cl is applied to the surface of the particles of the initial ZnO powder under CSP conditions at temperatures of 240–255 °C, pressing pressure of 396 MPa for 60 min, two processes characteristic of sintering ceramics are observed, namely: grain growth and an increase in the density of the initial powder backfill.

For dense ZnO ceramics formation, a sufficient level of activator content is required, depending on the additive type. Zinc acetate is a more active additive than ammonium chloride and, under the described conditions, leads to sufficient solid-phase mobility of ZnO crystals for CSP already at 0.927 mol%. To start the crystals' coalescence in the medium with ammonium chloride under the described conditions, about 7.6 mol% NH_4Cl is required. The type of activating additive also determines the mechanical pressing pressure required for CSP. During cold sintering in an acetate medium, the mode described in [14] was used, in which the powder is first compacted without heating at increased mechanical pressure (396 MPa), then the pressing pressure is reduced to 77 MPa, and CSP is carried out at a given temperature. It turned out that in an aqueous medium with the addition of 4.56 mol% and 7.6 mol% NH_4Cl, CSP occurs at an increased mechanical pressure of 396 MPa, i.e., without lowering the pressure after compaction of the powder backfill at room temperature. CSP with the addition of NH_4Cl requires optimization of conditions and modes to achieve the same values of relative density and grain size as CSP using zinc acetate. Simultaneously, the activating additive NH_4Cl potentially has an advantage in limiting ZnO ceramics' grain growth.

Analysis of the grain and crystal size distribution (Figure 6) shows that the close characteristics of the selected fine-dispersed component of the grain distribution of CSP samples and crystals of TVT samples indicate a similar mechanism of its formation. The presence of fine components of the crystal size distribution after TVT and grains after CSP may indicate a slight influence of the dissolution-precipitation mechanism on the processes under consideration. Since, otherwise, the proportion of fine components should not only increase compared to the original fine-crystalline powder (Figure 3) but, on the contrary, should decrease.

Under TVT conditions in the absence of mechanical pressure, the crystal size increases slightly with growth due to the surface spreading of the mass of mobile crystals. When adding mechanical pressure to CSP, under similar conditions, the probability of coalescence of crystals with solid-phase mobility of the structure increases. In this case, both a faster growth of crystalline grains and their compaction with forming a microstructure characteristic of ZnO ceramics are observed. A summary of the results of a comparative

study of CSP and TVT of a fine-crystalline ZnO powder with zinc acetate and ammonium chloride additives previously applied to the surface is schematically presented in Figure 8.
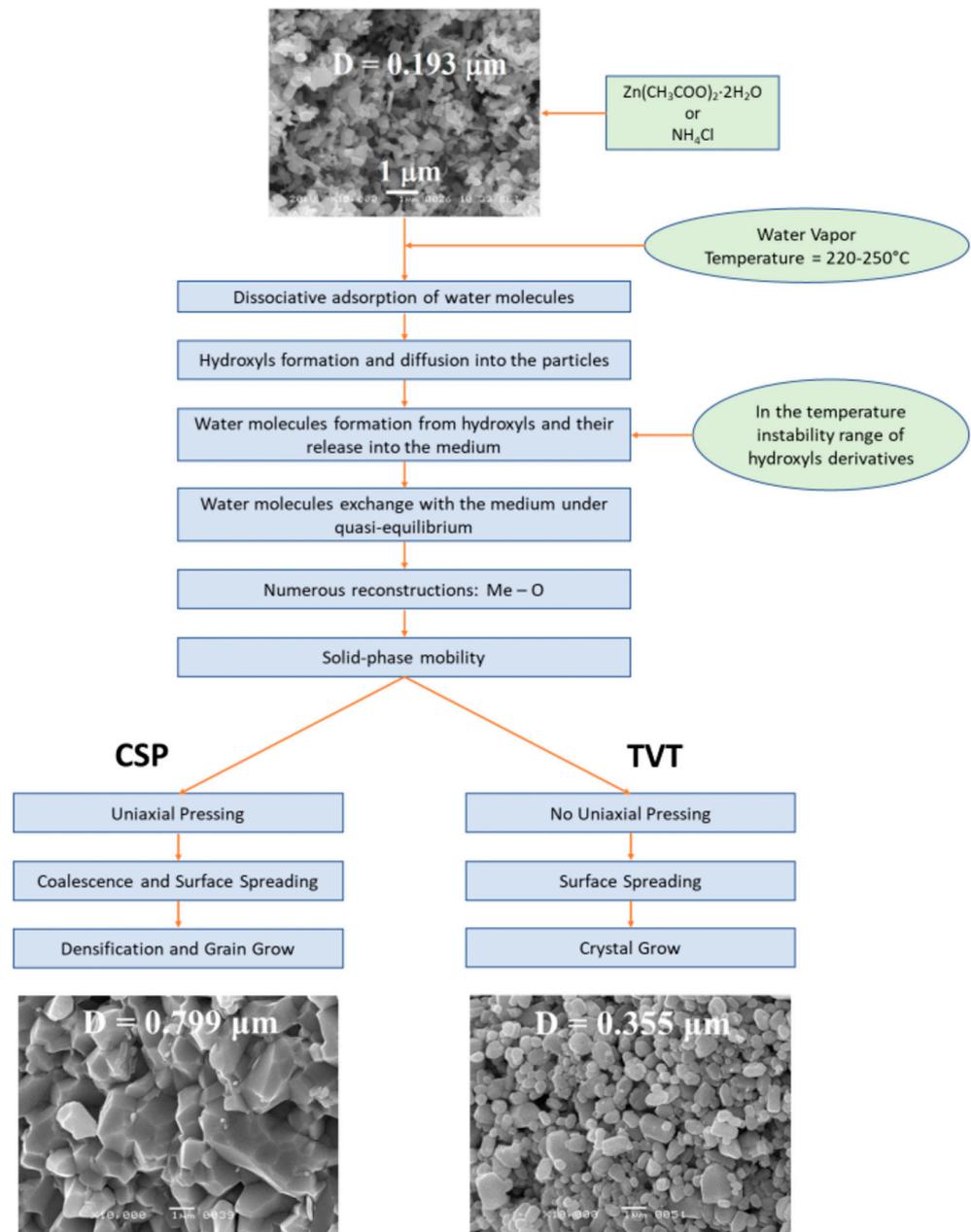

Figure 8. Scheme of the interaction of ZnO crystals with water vapor in the presence of activating additives in the CSP and TVT processes.

The initial stage of interaction is dissociative adsorption of water molecules [40–44], which leads to hydroxylation of the oxide and disordering of its structure. The resulting hydroxyl groups diffuse into the particle volume. It is assumed that rapid diffusion occurs due to the jump of protons over oxygen ions, both with and without breaking the metal-oxygen bond [45,46]. With the accumulation of hydroxyls, dehydroxylation begins with the formation and release of water molecules into the environment. The dehydroxylation stage occurs in the case of thermal instability of hydroxide compounds in the considered temperature range of transformations. In the study of hydroxylation and dehydroxylation of ZnO in a water medium, an essential role of proton transport at the interface and in adjacent layers was established [45]. The ratio of the hydroxylation

and dehydroxylation stages determines the concentration of hydroxyls in the particle volume. When the velocities of hydroxylation and dihydroxylation processes become approximately equal, a quasi-equilibrium of the particle with the medium is established. In this case, depending on the temperature, there is a more or less intensive exchange of water molecules between the water bound in the particle's structure and the environment. The result of the exchange of water molecules is numerous local rearrangements of the structure due to the break and restoration of Me–O bonds and the formation of defects and disordering of the structure. The formation of defects and local rearrangements of the structure determines the solid-phase mobility. The more intensive the exchange–the higher the mobility of the structure. The mobility of the surface layer and the volume of the particle should be different. The activating additive in the medium or on the interface affects the hydroxylation, the intensity of the exchange of water molecules, and the degree of solid-phase mobility of the oxide structure.

In the changes of the structure during dehydroxylation local regions that are coherent to the oxide lattice and more defective appear. Defective ones have a lower stability lifetime and are rebuilt more often. As a result, more stable regions accumulate, and the number of defective regions decreases, resulting in an oxide structure ordering. Ordering of the structure leads to a decrease in the content of hydroxyls and the intensity of exchange of water molecules with the medium, leading to a decrease in solid-phase mobility. Due to this, the probability of mass transfer through the surface spreading mechanism decreases. As a result, during the TVT process, crystals morphology changes, and the initial ZnO crystals' size increases up to a certain limit.

The application of mechanical pressure at CSP brings into contact individual particles of crystalline powder with solid-phase mobility. It increases the probability of coalescence of crystals. Simultaneously, two processes characteristic of sintering ceramics are observed: compaction of the initial powder backfill and grain growth.

5. Conclusions

Comparison of the results of changes in the dispersion of the initial ZnO powder with a crystal size of about 0.193 μm under CSP and TVT conditions at similar temperatures showed that in both processes, a mass transfer occurs in water vapor (in a low-density aqueous medium) according to the general mechanism of activation of the solid-phase mobility of the ZnO crystal structure. The mechanism of mass transfer by dissolution-precipitation does not play a dominant role in particle growth at TVT and the process of compaction and grain growth at CSP. This is due to the low content of the condensed liquid phase.

At the considered temperatures of TVT and CSP, activation of the solid-phase mobility occurs only in activating additives. At a low content of the additive, dense ceramics' formation occurs due to the shape changes of crystals with a mobile structure. An increase in the additive content above a certain threshold leads to coalescence of crystals and the ceramics grain growth. It is shown that the addition of 7.6 mol% ammonium chloride to the reaction medium causes the processes of compaction and grain growth similar to those observed in CSP ZnO with the addition of 0.925 mol% zinc acetate ions. Ammonium chloride has a weaker activating effect.

In an aqueous acetate medium, the ceramic grain size and relative density increase from 0.244 to 0.799 μm and from 0.83 to 0.96, respectively, in proportion to the activating additive amount. In an aqueous medium with the addition of ammonium chloride, the grain size of ceramics varies from 0.264 to 0.382 μm, the relative density from 0.82 to 0.91 with an increase in the content of the additive from 4.56 to 7.6 mol%. When zinc oxide is processed in water vapor at 240 °C without mechanical pressure, mass transfer by the surface spreading mechanism occurs, and a fine crystalline powder with crystal sizes from 0.316 to 0.355 μm is formed when activated by an acetate additive and from 0.383 to 0.386 μm when ammonium chloride is added.

The experimental results allow to make the conclusion about the possibility of choosing an activating additive for CSP based on data on the study of the effect of activators on the crystal growth of various oxides at TVT.

Author Contributions: Conceptualization, Y.I., A.S.; methodology, Y.I.; experimental investigation, Y.I., A.S., M.K. (Maxim Kornyushin); resources, M.K. (Mikhail Kormilicin); data analysis, Y.I., A.S., A.K.; writing—original draft preparation, Y.I., A.S., A.V.; writing—review and editing, V.S. All authors have read and agree to the published version of the manuscript.

Conflicts of Interest: The authors declare no conflict of interest.

References

1. Guo, H.; Baker, A.; Guo, J.; Randall, C.A. Protocol for Ultralow-Temperature Ceramic Sintering: An Integration of Nanotechnology and the Cold Sintering Process. *ACS Nano* **2016**, *10*, 10606–10614. [CrossRef] [PubMed]
2. Guo, H.; Guo, J.; Baker, A.; Randall, C.A. Hydrothermal-Assisted Cold Sintering Process: A New Guidance for Low-Temperature Ceramic Sintering. *ACS Appl. Mater. Interfaces* **2016**, *8*, 20909–20915. [CrossRef] [PubMed]
3. Maria, J.-P.; Kang, X.; Floyd, R.; Dickey, E.C.; Guo, H.; Guo, J.; Baker, A.; Funihashi, S.; Randall, C.A. Cold sintering: Current status and prospects. *J. Mater. Res.* **2017**, *32*, 3205–3218. [CrossRef]
4. Chaim, R.; Levin, M.; Shlayer, A.; Estournès, C. Sintering and densification of nanocrystalline ceramic oxide powders: A review. *Adv. Appl. Ceram.* **2008**, *107*, 159–169. [CrossRef]
5. Chen, P.-L.; Chen, I.-W. Sintering of Fine Oxide Powders: II, Sintering Mechanisms. *J. Am. Ceram. Soc.* **1997**, *80*, 637–645. [CrossRef]
6. Funahashi, S.; Guo, J.; Guo, H.; Wang, K.; Baker, A.L.; Shiratsuyu, K.; Randall, C.A. Demonstration of the cold sintering process study for the densification and grain growth of ZnO ceramics. *J. Am. Ceram. Soc.* **2017**, *100*, 546–553. [CrossRef]
7. Guo, J.; Floyd, R.; Lowum, S.; Maria, J.-P.; De Beauvoir, T.H.; Seo, J.-H.; Randall, C.A. Cold Sintering: Progress, Challenges, and Future Opportunities. *Annu. Rev. Mater. Res.* **2019**, *49*, 275–295. [CrossRef]
8. Biesuz, M.; Taveri, G.; Duff, A.I.; Olevsky, E.; Zhu, D.; Hu, C.; Grasso, S. A theoretical analysis of cold sintering. *Adv. Appl. Ceram.* **2020**, *119*, 75–89. [CrossRef]
9. Ndayishimiye, A.; Sengul, M.Y.; Bang, S.H.; Tsuji, K.; Takashima, K.; De Beauvoir, T.H.; Denux, D.; Thibaud, J.-M.; Van Duin, A.C.; Elissalde, C.; et al. Comparing hydrothermal sintering and cold sintering process: Mechanisms, microstructure, kinetics and chemistry. *J. Eur. Ceram. Soc.* **2020**, *40*, 1312–1324. [CrossRef]
10. Kang, X.; Floyd, R.; Lowum, S.; Cabral, M.J.; Dickey, E.C.; Maria, J.-P. Mechanism studies of hydrothermal cold sintering of zinc oxide at near room temperature. *J. Am. Ceram. Soc.* **2019**, *102*, 4459–4469. [CrossRef]
11. Ndayishimiye, A.; Largeteau, A.; Mornet, S.; Duttine, M.; Dourges, M.-A.; Denux, D.; Verdier, M.; Gouné, M.; De Beauvoir, T.H.; Elissalde, C.; et al. Hydrothermal Sintering for Densification of Silica. Evidence for the Role of Water. *J. Eur. Ceram. Soc.* **2018**, *38*, 1860–1870. [CrossRef]
12. Guo, H.; Baker, A.; Guo, J.; Randall, C.A. Cold Sintering Process: A Novel Technique for Low-Temperature Ceramic Processing of Ferroelectrics. *J. Am. Ceram. Soc.* **2016**, *99*, 3489–3507. [CrossRef]
13. Dargatz, B.; Gonzalez-Julian, J.; Bram, M.; Shinoda, Y.; Wakai, F.; Guillon, O. FAST/SPS sintering of nanocrystalline zinc oxide—Part II: Abnormal grain growth, texture and grain anisotropy. *J. Eur. Ceram. Soc.* **2016**, *36*, 1221–1232. [CrossRef]
14. Dargatz, B.; Gonzalez-Julian, J.; Bram, M.; Jakes, P.; Besmehn, A.; Schade, L.; Röder, R.; Ronning, C.; Guillon, O. FAST/SPS sintering of nanocrystalline zinc oxide—Part I: Enhanced densification and formation of hydrogen-related defects in presence of adsorbed water. *J. Eur. Ceram. Soc.* **2016**, *36*, 1207–1220. [CrossRef]
15. Gonzalez-Julian, J.; Neuhaus, K.; Bernemann, M.; Da Silva, J.P.; Laptev, A.; Bram, M.; Guillon, O. Unveiling the mechanisms of cold sintering of ZnO at 250 °C by varying applied stress and characterizing grain boundaries by Kelvin Probe Force Microscopy. *Acta Mater.* **2018**, *144*, 116–128. [CrossRef]
16. Grasso, S.; Biesuz, M.; Zoli, L.; Taveri, G.; Duff, A.I.; Ke, D.; Jiang, A.; Reece, M.J. A review of cold sintering processes. *Adv. Appl. Ceram.* **2020**, *119*, 115–143. [CrossRef]
17. Ivakin, Y.; Danchevskaya, M.; Kholodkova, A.; Muravieva, G.; Rybalchenko, V. Recrystallization of fine-crystalline barium titanate in low-density water medium. *J. Supercrit. Fluids* **2020**, *159*, 104771. [CrossRef]
18. Ivakin, Y.D.; Danchevskaya, M.N. Analysis of Recrystallization of Fine-Crystalline Corundum in a Supercritical Water Medium Using the Lognormal Particle Size Distribution Function. *Russ. J. Phys. Chem. B* **2018**, *12*, 1205–1211. [CrossRef]

19. Ivakin, Y.D.; Danchevskaya, M.N.; Muravieva, G.P. Recrystallization of Zinc Oxide in a Sub- and Supercritical Water Medium. *Russ. J. Phys. Chem. B* **2019**, *13*, 1189–1200. [CrossRef]

20. Bagwell, R.B.; Messing, G.L. Effect of Seeding and Water Vapor on the Nucleation and Growth of α-Al2O3 from γ-Al2O3. *J. Am. Ceram. Soc.* **1999**, *82*, 825–832. [CrossRef]

21. Lazarev, V.B.; Panasyuk, G.P.; Voroshilov, I.L.; Boudova, G.P.; Danchevskaya, M.N.; Torbin, S.N.; Ivakin, Y.D. New Ecologically Pure Technologies of Fine-Crystalline Materials. *Ind. Eng. Chem. Res.* **1996**, *35*, 3721–3725. [CrossRef]

22. Danchevskaya, M.; Torbin, S.; Muravieva, G.; Ovchinnikova, O.; Ivakin, Y. Synthesis and investigation of crystalline modifications of silicon dioxide. *React. Solids* **1988**, *5*, 293–303. [CrossRef]

23. Danchevskaya, M.N.; Ivakin, Y.D.; Torbin, S.N.; Panasyuk, G.P.; Belan, V.N.; Voroshilov, I.L. Scientific basis of technology of fine-crystalline quartz and corundum. *High Press. Res.* **2001**, *20*, 229–239. [CrossRef]

24. Branson, D.L. Kinetics and Mechanism of the Reaction Between Zinc Oxide and Aluminum Oxide. *J. Am. Ceram. Soc.* **1965**, *48*, 591–595. [CrossRef]

25. Ivakin, Y.D.; Danchevskaya, M.N.; Ovchinnikova, O.G.; Muravieva, G.P. Thermovaporous synthesis of fine crystalline gahnite ($ZnAl_2O_4$). *J. Mater. Sci.* **2006**, *41*, 1377–1383. [CrossRef]

26. Kholodkova, A.; Danchevskaya, M.; Ivakin, Y.; Smirnov, A.; Ponomarev, S.; Fionov, A.; Kolesov, V. Solid state synthesis of barium titanate in air and in supercritical water: Properties of powder and ceramics. *Ceram. Int.* **2019**, *45*, 23050–23060. [CrossRef]

27. Cunha-Duncan, F.N.; Bradt, R.C. Synthesis of Magnesium Aluminate Spinels from Bauxites and Magnesias. *J. Am. Ceram. Soc.* **2004**, *85*, 2995–3003. [CrossRef]

28. Yang, L.; Xiao, G.; Ding, D.; Li, P.; Lv, L.H.; Yang, S.L. Soild-phase synthesis of MgAl2O4 powder in reducing atmosphere: Effects of alumina sources and addition of carbon black. *Mater. Res. Express* **2019**, *6*, 045007. [CrossRef]

29. Danchevskaya, M.N.; Ivakin Yu., D.; Muravieva, G.P. Synthetic Magnesium Spinel—Raw Material for Optical Ceramics. In Proceedings of the 14th European Meeting on Supercritical Fluids, Marseille, France, 18–21 May 2014.

30. Kayani, Z.N.; Saleemi, F.; Batool, I. Effect of calcination temperature on the properties of ZnO nanoparticles. *Appl. Phys. A* **2015**, *119*, 713–720. [CrossRef]

31. Wang, M.; Zhou, Y.; Zhang, Y.; Hahn, S.H.; Kim, E.J. From $Zn(OH)_2$ to ZnO: A study on the mechanism of phase transformation. *CrystEngComm* **2011**, *13*, 6024–6026. [CrossRef]

32. Mukhopadhyay, S.; Das, P.P.; Maity, S.; Ghosh, P.; Devi, P.S. Solution grown ZnO rods: Synthesis, characterization and defect mediated photocatalytic activity. *Appl. Catal. B Environ.* **2015**, *165*, 128–138. [CrossRef]

33. Ivakin, Y.D.; Smirnov, A.V.; Tarasovskii, V.P.; Rybal'Chenko, V.V.; Vasin, A.A.; Kholodkova, A.A.; Kormilitsin, M.N. Cold Sintering of ZnO Ceramic in Water Medium: Test Demonstration. *Glas. Ceram.* **2019**, *76*, 210–215. [CrossRef]

34. Egbuchunam, T.; Balkose, D. Effect of Supercritical Ethanol Drying on the Properties of Zinc Oxide Nanoparticles. *Dry. Technol.* **2012**, *30*, 739–749. [CrossRef]

35. Vukalovich, M.P.; Rivkin, S.L. *Thermophysical Properties of Water and Water Vapor*; Mashinostroyeniye: Moscow, Russia, 1967; pp. 1–160.

36. Ali, M.; Winterer, M. ZnO Nanocrystals: Surprisingly 'Alive'. *Chem. Mater.* **2010**, *22*, 85–91. [CrossRef]

37. Thurber, A.P.; Alanko, G.A.; Beausoleil, G.L.; Dodge, K.N.; Hanna, C.B.; Punnoose, A. Unusual crystallite growth and modification of ferromagnetism due to aging in pure and doped ZnO nanoparticles. *J. Appl. Phys.* **2012**, *111*, 7. [CrossRef]

38. Nie, J.; Zhang, Y.; Chan, J.M.; Huang, R.; Luo, J. Water-assisted flash sintering: Flashing ZnO at room temperature to achieve ~98% density in seconds. *Scr. Mater.* **2018**, *142*, 79–82. [CrossRef]

39. Dargatz, B.; Gonzalez-Julian, J.; Guillon, O. Anomalous coarsening of nanocrystalline zinc oxide particles in humid air. *J. Cryst. Growth* **2015**, *419*, 69–78. [CrossRef]

40. Meyer, B.; Marx, D.; Dulub, O.; Diebold, U.; Kunat, M.; Langenberg, D.; Wöll, C. Partial Dissociation of Water Leads to Stable Superstructures on the Surface of Zinc Oxide. *Angew. Chem. Int. Ed.* **2004**, *43*, 6641–6645. [CrossRef]

41. Wang, Y.; Muhler, M.; Wöll, C.; Wöll, C. Spectroscopic evidence for the partial dissociation of H_2O on ZnO($10\bar{1}0$). *Phys. Chem. Chem. Phys.* **2006**, *8*, 1521–1524. [CrossRef]

42. Kenmoe, S.; Biedermann, P.U. Water aggregation and dissociation on the ZnO($10\bar{1}0$) surface. *Phys. Chem. Chem. Phys.* **2017**, *19*, 1466–1486. [CrossRef]

43. Newberg, J.T.; Goodwin, C.; Arble, C.; Khalifa, Y.; Boscoboinik, J.A.; Rani, S. ZnO($10\bar{1}0$) Surface Hydroxylation under Ambient Water Vapor. *J. Phys. Chem. B* **2017**, *122*, 472–478. [CrossRef] [PubMed]

44. Yu, X.; Schwarz, P.; Nefedov, A.; Meyer, B.; Wang, Y.; Wöll, C. Structural Evolution of Water on ZnO(100): From Isolated Monomers via Anisotropic H-Bonded 2D and 3D Structures to Isotropic Multilayers. *Angew. Chem. Int. Ed.* **2019**, *58*, 17751–17757. [CrossRef] [PubMed]

45. Quaranta, V.; Hellström, M.; Behler, J. Proton-Transfer Mechanisms at the Water–ZnO Interface: The Role of Presolvation. *J. Phys. Chem. Lett.* **2017**, *8*, 1476–1483. [CrossRef] [PubMed]

46. Ramabhadran, R.O.; Mayhall, N.J.; Raghavachari, K. Proton Hop Paving the Way for Hydroxyl Migration: Theoretical Elucidation of Fluxionality in Transition-Metal Oxide Clusters. *J. Phys. Chem. Lett.* **2010**, *1*, 3066–3071. [CrossRef]